CGI-58/ABHD5-Derived Signaling Lipids Regulate Systemic Inflammation and Insulin Action

Caleb C. Lord,[1] Jenna L. Betters,[1] Pavlina T. Ivanova,[2] Stephen B. Milne,[2] David S. Myers,[2] Jennifer Madenspacher,[3] Gwynneth Thomas,[1] Soonkyu Chung,[1] Mingxia Liu,[1] Matthew A. Davis,[1] Richard G. Lee,[4] Rosanne M. Crooke,[4] Mark J. Graham,[4] John S. Parks,[1] Dawn L. Brasaemle,[5] Michael B. Fessler,[3] H. Alex Brown,[2] and J. Mark Brown[1]

Mutations of comparative gene identification 58 (CGI-58) in humans cause Chanarin-Dorfman syndrome, a rare autosomal recessive disease in which excess triacylglycerol (TAG) accumulates in multiple tissues. CGI-58 recently has been ascribed two distinct biochemical activities, including coactivation of adipose triglyceride lipase and acylation of lysophosphatidic acid (LPA). It is noteworthy that both the substrate (LPA) and the product (phosphatidic acid) of the LPA acyltransferase reaction are well-known signaling lipids. Therefore, we hypothesized that CGI-58 is involved in generating lipid mediators that regulate TAG metabolism and insulin sensitivity. Here, we show that CGI-58 is required for the generation of signaling lipids in response to inflammatory stimuli and that lipid second messengers generated by CGI-58 play a critical role in maintaining the balance between inflammation and insulin action. Furthermore, we show that CGI-58 is necessary for maximal T_H1 cytokine signaling in the liver. This novel role for CGI-58 in cytokine signaling may explain why diminished CGI-58 expression causes severe hepatic lipid accumulation yet paradoxically improves hepatic insulin action. Collectively, these findings establish that CGI-58 provides a novel source of signaling lipids. These findings contribute insight into the basic mechanisms linking T_H1 cytokine signaling to nutrient metabolism. ***Diabetes*** **61:355–363, 2012**

Comparative gene identification 58 (CGI-58), also known as α/β hydrolase domain-containing protein 5 (ABHD5), recently has gained attention as the master regulator of triacylglycerol (TAG) hydrolysis and phospholipid metabolism (1–4). However, molecular mechanisms by which CGI-58 regulates these metabolic processes still are incompletely understood. Because the discovery that mutations in CGI-58 cause Chanarin-Dorfman syndrome (CDS) (5), several groups have studied CGI-58's biochemical properties in vitro (1–4). An important advancement on this front came when it was demonstrated that CGI-58 indirectly promotes TAG hydrolysis by coactivating adipose triglyceride lipase (ATGL) (1). However, recent studies in mice with diminished levels of CGI-58 clearly show that ATGL-independent functions for CGI-58 also must exist (2,6). In addition to activating ATGL, CGI-58 catalyzes the acylation of lysophosphatidic acid (LPA) to generate the critical lipid second messenger phosphatidic acid (PA). Both the substrate (LPA) and the product (PA) of the LPA acyltransferase (LPAAT) reaction are well-known signaling lipids with critical roles in angiogenesis, cardiac development, carcinogenesis, and immunity (7–9). Furthermore, fibroblasts from CDS patients have dramatically altered rates of synthesis and turnover of other major lipids with signaling potential, including phosphatidylcholine (PC), phosphatidylinositol, and phosphatidylserine (10,11). Given the central importance of lipid mediators in growth factor and cytokine-mediated signal transduction (7–9), we reasoned that CGI-58 may be a novel source of signaling lipids. Unfortunately, conventional gene targeting of CGI-58 in mice results in premature lethality (6). To circumvent this, we used targeted antisense oligonucleotides (ASOs) to test whether CGI-58 plays a quantitatively important role in the generation of signaling lipids in vivo. Our findings show that CGI-58 is a novel source of signaling lipids that links inflammation to TAG and glucose metabolism.

RESEARCH DESIGN AND METHODS

Male C57BL/6N mice (Harlan) were maintained on standard rodent chow or a high-fat diet (HFD) for a period of 4–10 weeks and simultaneously injected with ASOs targeting knockdown (KD) of CGI-58, as previously described (2). The diets and ASOs used here have been described elsewhere (2). The HFD was prepared by our institutional diet core and contains ~45% of energy as lard (16:0 = 23.3, 18:0 = 15.9, 18:1 = 34.8, and 18:2 = 18.7%). The 20-mer phosphorothioate ASOs were designed to contain 2'-0-methoxyethyl groups at positions 1–5 and 15–20 and were synthesized, screened, and purified, as described previously (12), by ISIS Pharmaceuticals (Carlsbad, CA). The CGI-58 ASOs used in the current studies were described as CGI-58 ASO^{β} in our previous work (2). All mice were maintained in an American Association for Accreditation of Laboratory Animal Care–approved specific pathogen-free environment on a 12:12-h light:dark cycle and allowed free access to regular chow and water. All experiments were performed with the approval of the institutional animal care and use committee.

Lipopolysaccharide-induced acute-phase response. Mice were injected with control or CGI-58 ASOs and maintained on standard chow or an HFD for a period of 4 weeks, as previously described (2). After 4 weeks of ASO treatment, mice were injected intraperitoneally with either saline or 5 μg lipopolysaccharide (LPS) (*Escherichia coli* 0111:B4). Following injection, plasma was collected at 1 h by submandibular puncture (for tumor necrosis factor [TNF] α measurements), and exactly 6 h after injection mice were killed with ketamine/xylazine (100–160 mg/kg ketamine and 20–32 mg/kg xylazine). Thereafter, a midline laparotomy was performed, and blood was collected by heart puncture. After blood collection, a whole-body perfusion was conducted by puncturing the inferior vena cava and slowly delivering 10 mL sterile 0.9% saline into the left ventricle of the heart to remove residual blood. Multiple tissues were collected and snap-frozen for subsequent analysis.

From the [1]Department of Pathology, Section on Lipid Sciences, Wake Forest University School of Medicine, Winston-Salem, North Carolina; the [2]Department of Pharmacology, Vanderbilt University School of Medicine, Nashville, Tennessee; the [3]Laboratory of Respiratory Biology, National Institute of Environmental Health Sciences, Research Triangle Park, North Carolina; the [4]Cardiovascular Group, Antisense Drug Discovery, Isis Pharmaceuticals, Carlsbad, California; and the [5]Department of Nutritional Sciences, Rutgers, The State University of New Jersey, New Brunswick, New Jersey.
Corresponding author: J. Mark Brown, mabrown@wakehealth.edu.
Received 18 July 2011 and accepted 19 November 2011.
DOI: 10.2337/db11-0994
This article contains Supplementary Data online at http://diabetes.diabetesjournals.org/lookup/suppl/doi:10.2337/db11-0994/-/DC1.

In vivo insulin-signaling analyses. Mice were injected with control or CGI-58 ASOs and maintained on standard chow or an HFD for a period of 8 weeks, as previously described (2). After an overnight fast (11:00 P.M. to 9:00 A.M.), mice were anesthetized with isoflurane (4% for induction and 2% for maintenance) and were maintained on a 37°C heating pad to control body temperature. A minimal midline laparotomy was performed, and the portal vein was visualized. Sterile saline or recombinant human insulin (0.5 units/kg body wt; Novo Nordisk) was administered directly into the portal vein. Exactly 5 min later, tissues were excised without saline perfusion and immediately snap frozen in liquid nitrogen. Protein extracts from tissues were analyzed by Western blotting, as previously described (13–15).

In vivo hepatic TNFα-signaling analyses. Mice were injected with control or CGI-58 ASOs and maintained on standard chow or an HFD for a period of 4 weeks, as previously described (2). After an overnight fast (11:00 P.M. to 9:00 A.M.), mice were anesthetized with isoflurane (4% for induction and 2% for maintenance) and were maintained on a 37°C heating pad to control body temperature. A minimal midline laparotomy was performed, and the portal vein was visualized. Saline or mouse recombinant TNFα (10 ng/mouse, no. 410-MT; R&D Systems) was administered directly into the portal vein. Exactly 5 min later, the liver was excised without saline perfusion and immediately snap-frozen in liquid nitrogen. Protein extracts from tissues were analyzed by Western blotting, as previously described (13–15), and lipid extracts were analyzed using mass spectrometry methods (16), as described in detail below.

Cytokine signaling in primary hepatocytes. After 4 weeks of ASO treatment, mouse primary hepatocytes were isolated by collagenase perfusion from chow-fed mice, as previously described (17). Hepatocytes were cultured for 3–6 h to dampen serum-driven signaling and then stimulated with recombinant mouse TNFα (100 ng/mL, no. 410-MT; R&D Systems), interleukin (IL)-1β (10 ng/mL, no. 401-ML; R&D Systems), or IL-6 (10 ng/mL, no. 406-ML/CF; R&D Systems) over an acute time course. Protein extracts from tissues were analyzed by Western blotting for phospho–c-Jun NH_2-terminal kinase (*p*-JNK; Thr183/Tyr185), phospho-S6 ribosomal protein (*p*-S6; Ser235/236), and β-actin, as previously described (13–15).

Plasma biochemistries. Detailed descriptions of plasma lipid and lipoprotein analyses have been previously described (14,15). Plasma cytokines were quantified by multiplex assay (Bio-Plex; Bio-Rad) as previously described (18). In some cases (Fig. 4*A*), the level of plasma TNFα was determined by enzyme-linked immunosorbent assay (no. MTA00; R&D Systems).

LPA acyltransferase activity assay. Whole-liver homogenates were prepared from snap-frozen mouse liver by dounce homogenization in 50 mmol/L Tris, pH 7.5; 300 mmol/L NaCl; 50 mmol/L NaF; and Sigma protease inhibitor cocktail just before the assay. Cellular debris was removed by centrifugation at 1,000*g* for 15 min at 4°C, and the supernatant was used for determination of protein content by Lowry assay (19). Total hepatic LPAAT activity was determined by measuring the conversion of [1-^{14}C]-oleoyl-CoA to [1-^{14}C]-PA, as previously described (3). The reaction was assembled in 100 μL of 50 mmol/L Tris (pH 7.5) containing 50 μmol/L oleoyl-*sn*1-glycerol-3-phosphate (Avanti Polar Lipids, Alabaster, AL) and 10 μmol/L [1-^{14}C]-oleoyl-CoA (specific activity 8,000 dpm/nmol) using 5 μg of whole-liver homogenate and continued for 10 min at 30°C.

Immunoblotting. Whole-tissue homogenates were made from multiple tissues in a modified radioimmunoprecipitation assay buffer, as previously described (13–15). Proteins were separated by 4–12% SDS-PAGE and transferred to polyvinylidene difluoride membranes, and proteins were detected after incubation with specific antibodies. Information on the antibodies used is available upon request.

Hepatic neutral lipid and glycerophospholipid analyses. Extraction of liver lipids for enzymatic quantification of total TAG, cholesteryl esters (14,15), free cholesterol, and phospholipid was performed as previously described. Glycerophospholipids were extracted using a modified Bligh and Dyer procedure (20). Approximately 10 mg of frozen mouse liver was homogenized in 800 μL ice-cold 0.1 N HCl:CH_3OH (1:1) using a tight-fit glass homogenizer (Kimble/Kontes Glass, Vineland, NJ) for ~1 min on ice. Suspension was then transferred to cold 1.5-mL microfuge tubes (Laboratory Product Sales, Rochester, NY) and vortexed with 400 μL cold $CHCl_3$ for 1 min. The extraction proceeded with centrifugation (5 min, 4°C, 18,000*g*) to separate the two phases. The lower organic layer was collected and the solvent was evaporated. The resulting lipid film was dissolved in 100 μL isopropanol:hexane:100 mmol/L NH_4CO_2H(aq) (58:40:2) (mobile phase A). Quantification of glycerophospholipids was achieved by the use of a liquid chromatography–mass spectrometry technique using synthetic (non–naturally occurring) diacyl and lysophospholipid standards. Typically, 200 ng of each odd-carbon standard was added per 10–20 mg tissue. Glycerophospholipids were analyzed on an Applied Biosystems/MDS SCIEX 4000 Q TRAP hybrid triple quadrupole/linear ion trap mass spectrometer (Applied Biosystems, Foster City, CA) and a Shimadzu high-pressure liquid chromatography system with a Phenomenex Luna Silica column (2 × 250 mm, 5-μm particle size) using a gradient elution, as previously described (16). The identification of the individual species, achieved by liquid chromatography–tandem mass spectrometry, was based on their chromatographic and mass spectral characteristic. This analysis allows identification of the two fatty acid moieties but does not determine their position on the glycerol backbone (*sn-1* vs. *sn-2*). TAG, diacylglycerol (DAG), and monoacylglycerol (MAG) from frozen mouse liver tissue (10–15 mg) were extracted by homogenizing tissue in the presence of internal standards (500 ng each of 14:0 MAG, 24:0 DAG, and 42:0 TAG) in 2 mL 1× PBS and extracting with 2 mL ethyl acetate: trimethylpentane (25:75). After drying the extracts, the lipid film was dissolved in 1 mL hexane:isopropanol (4:1) and passed through a bed of Silicagel 60 Å to remove the remaining polar phospholipids. Solvent from the collected fractions was evaporated and lipid film was redissolved in 100 μL CH_3OH:$CHCl_3$ (9:1), containing 10 μL of 100 mmol/L CH_3COONa for mass spectrometry analysis, essentially as described previously (21).

Quantitative real-time PCR. Tissue RNA extraction and quantitative real-time PCR (qPCR) was conducted as previously described (14,15). Cyclophilin or hypoxanthine phosphoribosyltransferase 1 was used as invariant controls for these studies, and expression levels were calculated based on the $\Delta\Delta C_T$ method. qPCR was conducted using the Applied Biosystems 7500 Real-Time PCR System. Primers used for qPCR are available on request.

Statistical analysis. All data are expressed as means ± SEM and were analyzed using either a one-way or two-way ANOVA followed by Student *t* tests for post hoc analysis using JMP version 5.0.12 software (SAS Institute, Inc., Cary, NC).

RESULTS

CGI-58 KD paradoxically improves hepatic insulin signaling. Our original interest in CGI-58's role in intracellular signaling was sparked by the unexplained "metabolic paradox" apparent in mice with diminished CGI-58 function (Fig. 1). We have discovered that CGI-58 KD results in striking hepatic steatosis (Fig. 1*A*) (2) yet paradoxically improves systemic glucose and insulin tolerance (2). It is well accepted that hepatic lipotoxicity, and more specifically the hepatic accumulation of signaling lipids such as DAG and ceramides, is linked to insulin resistance (22). However, hepatic lipid insult is not sufficient to cause insulin resistance in CGI-58 ASO-treated mice (Fig. 1) (2). Instead, CGI-58 KD actually improves systemic insulin action despite these metabolic abnormalities (2). To confirm that the hepatic steatosis seen in CGI-58 ASO-treated mice were indeed dissociated from primary defects in insulin signaling, we analyzed acute Akt and FoxO1 phosphorylation in response to portally administered insulin (Fig. 1*B*–*G*). In agreement with previous measures of systemic glucose and insulin tolerance (2), CGI-58 KD significantly improved hepatic insulin signaling (Fig. 1*B* and *E*). CGI-58 KD had no significant impact on insulin-stimulated Akt phosphorylation in skeletal muscle (Fig. 1*C* and *F*) and adipose tissue (Fig. 1*D* and *G*). Collectively, these data have uncovered an unexpected role for CGI-58 in dissociating hepatic steatosis from insulin resistance. This prompted us to examine the molecular basis for this dissociation.

CGI-58 KD prevents HFD-induced hepatic stress kinase activation. CGI-58 ASO-treated mice have elevated hepatic levels of multiple lipid species, TAG (Supplementary Fig. 1), DAG (Supplementary Fig. 2), MAG (Supplementary Fig. 3), and ceramides (2), yet accumulation of these lipid intermediates is insufficient to cause local insulin resistance (Fig. 1*B* and *E*). Thus, other factors must overcome this lipid insult to improve insulin signaling in the liver. In addition to the lipid hypothesis of insulin resistance (22), chronic elevation of proinflammatory T_H1 cytokine action in metabolic tissues also promotes insulin resistance (23–28). It is noteworthy that both lipid- and cytokine-induced insulin resistance involve the chronic activation of stress kinase signaling pathways, such as IκB kinase β (IKKβ) (24,25), S6 kinase 1 (S6K1) (26), the

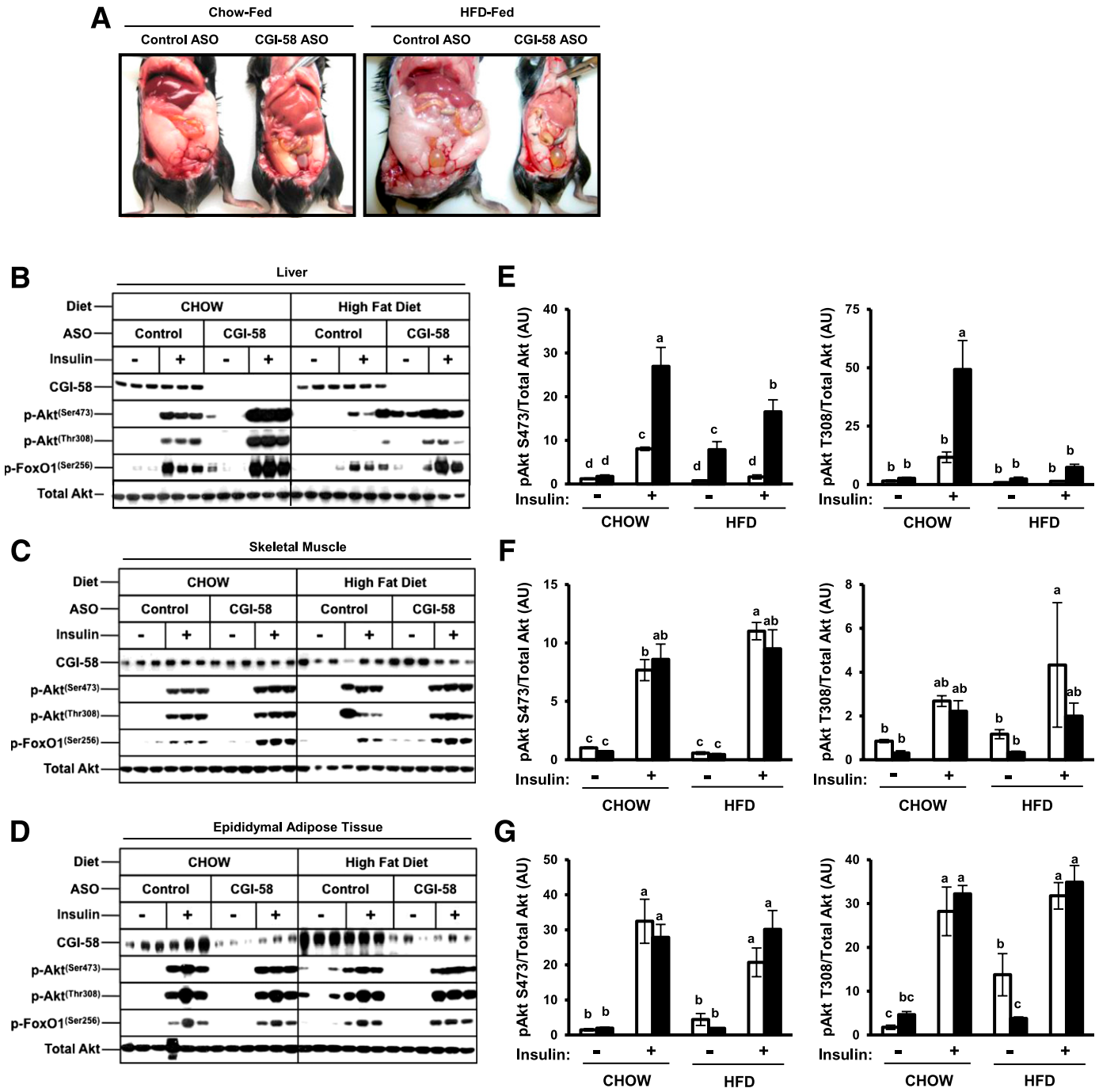

FIG. 1. CGI-58 KD dissociates hepatic steatosis from insulin resistance. *A*: Photographs depicting hepatic steatosis and adiposity in C57BL/6N mice fed either a chow or HFD for 10 weeks in conjunction with biweekly injections (25 mg/kg) of either a nontargeting control ASO or ASO targeting KD of CGI-58 (CGI-58 ASO). *B–G*: Despite hepatic lipid insult, KD of CGI-58 enhances insulin signaling. Mice were fed either a chow or HFD and treated with ASOs for 8 weeks. Mice were fasted for 10 h before saline or insulin injection into the portal vein. Exactly 5 min later, tissues were excised and immediately snap-frozen in liquid nitrogen. Protein extracts from the liver (*B*), skeletal muscle (*C*), and adipose tissue (*D*) were analyzed by Western blotting for total Akt, phospho (p)-Akt (Ser473 and Thr308), and phospho (p)-FoxO1 (Ser256); three representative animals are shown for each group. *E–G*: Densitometric analyses of insulin signaling: Phospho-Akt protein levels were normalized to total Akt in liver (*E*), skeletal muscle (*F*), and adipose tissue (*G*). □, control ASO; ■, CGI-58 ASO. Data represent the mean ± SEM from three mice per group, and values not sharing a common superscript letter differ significantly ($P < 0.05$). AU, arbitrary unit. (A high-quality digital representation of this figure is available in the online issue.)

mammalian target of rapamycin (mTOR) (26,27), and JNK (28), which dampen insulin signaling by phosphorylating serine residues of insulin receptor substrate (IRS) proteins (IRS-1 and IRS-2). Hence, we examined circulating levels of proinflammatory cytokines and the activation state of cytokine-induced stress kinases (IKKβ, S6K1, mTOR, and JNK) in metabolic tissues of CGI-58 ASO-treated mice (Fig. 2). CGI-58 KD caused modest elevations in the plasma levels of several proinflammatory cytokines (IL12p40; monocyte chemoattractant protein-1 (MCP-1); macrophage inflammatory protein-2 (MIP-2); CXCL1; regulated upon activation, normal T-cell expressed, and secreted

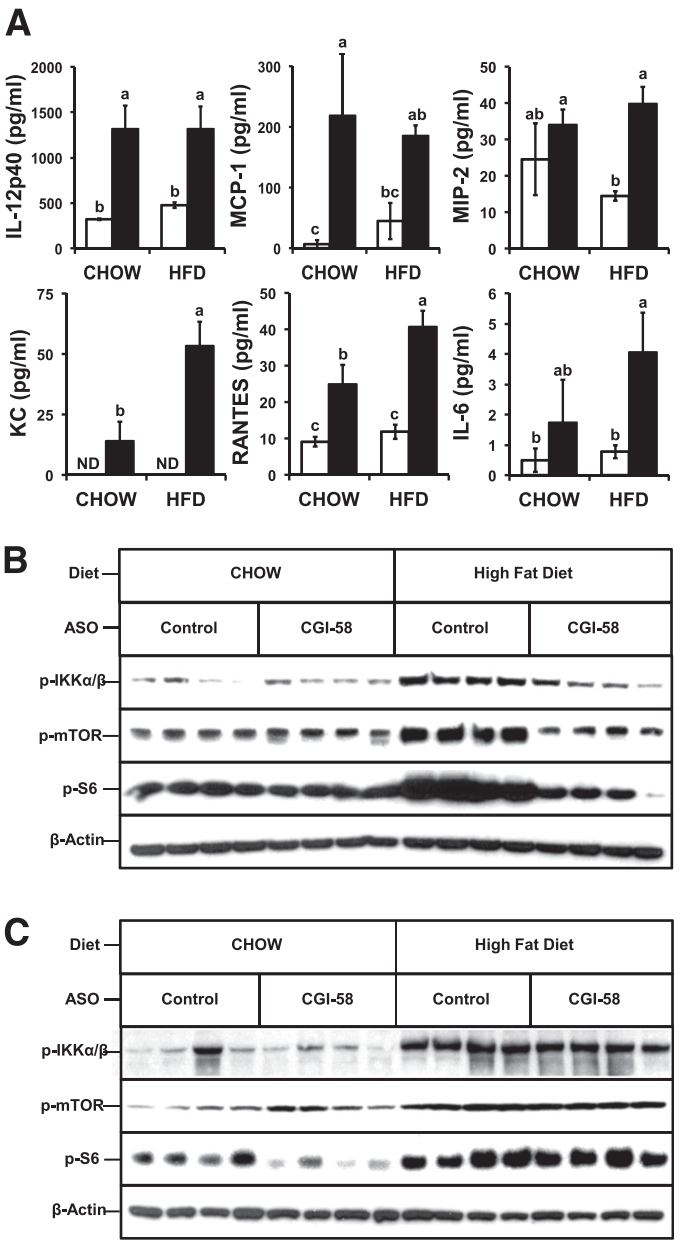

FIG. 2. CGI-58 KD alters HFD-induced inflammation: Evidence of hepatic cytokine resistance. C57BL/6N mice were fed either a standard chow or HFD in conjunction with biweekly injections of either a nontargeting control ASO (□) or ASO targeting KD of CGI-58 (CGI-58 ASO; ■) for 10 weeks. *A*: Plasma levels of proinflammatory cytokines, including IL-6 and IL-12p40; monocyte chemoattractant protein-1 (MCP-1); macrophage inflammatory protein-2 (MIP-2); CXCL1 (KC); and regulated upon activation, normal T-cell expressed, and RANTES. Data represent the mean ± SEM from five mice per group, and values not sharing a common superscript letter differ significantly ($P < 0.05$). ND, levels below limit of detection. *B* and *C*: HFD-induced stress kinase activation. Representative immunoblots from liver (*B*) or epididymal adipose tissue (*C*) are shown for phospho-IκB kinase α/β (p-IKKα/β; Ser176/180), phospho-mTOR (p-mTOR; Ser2448), and phospho-S6 ribosomal protein (p-S6; Ser235/236). Membranes were probed for β-actin and CGI-58 to serve as loading controls; data from four representative animals are shown for each group.

[RANTES]; and IL-6) in chow-fed mice, and several of these cytokines were further increased by HFD feeding (Fig. 2*A*). However, despite elevated circulating T_H1 cytokines (Fig. 2*A*), CGI-58 ASO-treated mice were completely protected against HFD-induced activation of stress kinases, such as IKKβ, S6K1, and mTOR, in the liver (Fig. 2*B*). In contrast, HFD-induced activation of these kinases was not altered in adipose tissue (Fig. 2*C*). CGI-58 KD also prevented HFD-induced serine phosphorylation of IRS-1 (Ser1101) in the liver (Supplementary Fig. 13*A* and *C*) but did not alter IRS-1 phosphorylation in adipose tissue (Supplementary Fig. 13*B* and *D*).

CGI-58 KD prevents maximal TNFα signaling in the liver. The LPAAT product (PA) is a known lipid second messenger generated acutely in response to TNFα (29), IL-1 (30), and lipid A (31) in cell models. Moreover, LPAAT inhibitors can blunt inflammatory cytokine action in models of sepsis (32) and acute lung injury (33). To further test whether CGI-58 could contribute to T_H1 cytokine signaling in the liver, we examined the generation of lipid second messengers and activation of downstream kinases in response to TNFα administration (Fig. 3). Hepatic TNFα signaling was interrogated based on its well-known ability to dampen insulin signaling (23) and promote TAG hydrolysis (34), two pathways that are regulated by CGI-58 in vivo (2,6). To examine acute TNFα signaling, we portally administered physiological levels of recombinant TNFα and analyzed signaling lipid generation at 5 min after stimulation. In control ASO-treated mice, TNFα treatment elicited a small (18%) but significant increase in hepatic total PA levels, compared with saline treatment (Fig. 3*A*). It is noteworthy that CGI-58 KD prevented TNFα-induced PA generation (Fig. 3*A*). Neither TNFα nor CGI-58 KD significantly altered total hepatic LPAAT activity (Fig. 3*B*), which was not surprising because multiple LPAAT enzymes are expressed in mouse liver (35). Of interest, CGI-58 KD specifically prevented TNFα-driven increases in 34:2 PA and 38:4 PA species (Fig. 3*A*), whereas other PA species were not altered (Supplementary Fig. 4). In addition, CGI-58 KD reduced basal levels of multiple hepatic glycerophospholipid species with signaling potential (36:4 PA, 34:1 PE, 34:2 PE, 36:1 PE, 36:2 PE, 36:4 PE, 36:2 PEp, 34:1 PC, 34:2 PC, and 40:6 PC) regardless of TNFα treatment (Supplementary Figs. 4–9). As previously reported (2), CGI-58 KD also caused large increases in hepatic phosphatidylglycerol levels, independent of TNFα treatment (Fig. 3*A* and Supplementary Fig. 10). Because TNFα signaling requires lipid second messengers (29), we examined whether CGI-58 KD blunted downstream signal transduction in the liver (Fig. 3*C*). Five minutes after TNFα administration in vivo, hepatic IκBα (a nuclear factor κB inhibitory protein) was hyperphosphorylated at serine 32 in control mice, whereas CGI-58 KD significantly attenuated hepatic IκBα phosphorylation (Fig. 3*C*). To determine whether the role of CGI-58 in hepatic cytokine action was cell autonomous, we isolated primary hepatocytes from CGI-58 ASO-treated mice. CGI-58 KD prevented JNK hyperphosphorylation and S6K1 activation in response to a time-course stimulation with TNFα (Fig. 3*D*), IL-1β (Fig. 3*E*), and IL-6 (Fig. 3*F*). Collectively, these data suggest that CGI-58–generated signaling lipids may participate in multiple cytokine signaling cascades, which deserves further exploration.

CGI-58 KD alters the systemic response to endotoxin. Although T_H1 cytokines (TNFα, IL-1β, and IL-6) clearly have been implicated in promoting chronic inflammatory conditions that accompany obesity (23–28), T_H1 cytokine action has been best characterized in models of acute inflammation driven by microbial infection or tissue injury (36,37). In acute inflammation, $T_H1$cytokines are produced transiently by macrophages and mast cells to promote

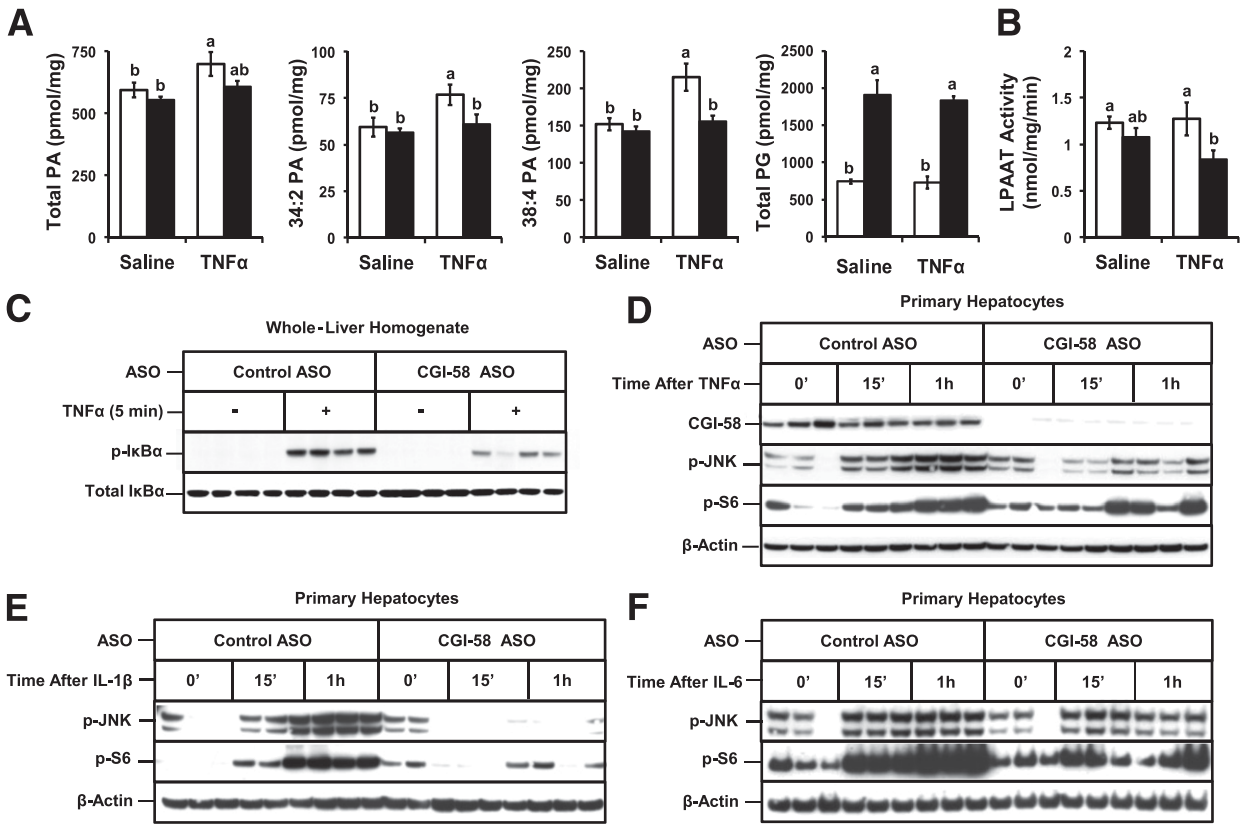

FIG. 3. CGI-58–generated signaling lipids are necessary for maximal TNFα signaling in the liver. *A–C*: Mice were maintained on a chow diet for 4 weeks in conjunction with biweekly injections (25 mg/kg) of either a nontargeting control ASO (□) or ASO targeting knockdown of CGI-58 (CGI-58 ASO; ■). Mice were fasted for 10 h before injection of saline or TNFα (10 ng) into the portal vein. Exactly 5 min later, the liver was excised and immediately snap-frozen in liquid nitrogen for signaling analyses. *A*: Hepatic levels of PA and phosphatidylglycerol (PG) were analyzed by mass spectrometry. *B*: Total hepatic LPAAT activity. Data in *A* and *B* represent the mean ± SEM from four mice per group, and values not sharing a common superscript letter differ significantly ($P < 0.05$). *C*: Protein extracts from the liver were analyzed for total IκB α (IκBα) and phospho-IκBα (p-IκBα; Ser32); data from four representative animals are shown for each group. *D–F*: Acute stress kinase activation in primary hepatocytes. Following 4 weeks of ASO treatment, hepatocytes were isolated from control and CGI-58 ASO-treated mice by collagenase perfusion. Freshly isolated hepatocytes were stimulated for 15 min (15') or 1 h with 100 ng/mL TNFα (*D*), 10 ng/mL IL-1β (*E*), or 10 ng/mL IL-6 (*F*). Downstream signaling was analyzed by immunoblotting for p-JNK (Thr183/Tyr185), phospho-S6 ribosomal protein (p-S6; Ser235/236), and β-actin. Data in *D–F* represent responses of hepatocytes isolated from three individual mice per condition.

tissue reprogramming typified by the hepatic acute-phase response (34,36,37). Of interest, the acute-phase response in the liver also is associated with transient overproduction of VLDL-TAG (34) and insulin resistance (24,25), two pathways that are stimulated by CGI-58 in vivo (2) (Figs. 1*D–F*). To test whether CGI-58 participates in cytokine action and TAG metabolism during acute inflammation, we injected CGI-58 ASO-treated mice with a low dose of LPS (*E. coli*). In response to LPS, CGI-58 KD significantly elevated plasma levels of TNFα, IL-6, and IL-12p40, compared with LPS-injected controls (Fig. 4*A*). Of note, 1 h after LPS injection, mice that received CGI-58 ASOs had fivefold more circulating TNFα than LPS-injected control mice (Fig. 4*A*). Despite the elevation in circulating T_H1 cytokines (Fig. 4*A*), LPS-induced expression of TNFα and markers of the acute-phase response (serum amyloid A [SAA] and serum amyloid P-component [SAP]) were significantly reduced in livers of CGI-58 ASO-treated mice (Fig. 4*B*). LPS-induced plasma levels of SAA and haptoglobin also were decreased in CGI-58 ASO-treated mice (Fig. 4*A*). However, LPS induced higher expression of other cytokines, such as IL-12p40 and IL-10, in the livers of CGI-58 ASO-treated mice (Fig. 4*B*). It is noteworthy that, in parallel to altered circulating levels of cytokines (Fig. 4*A*), LPS injection increased the expression of TNFα, IL-6, IL12p40, and IL-10 in adipose of CGI-58 ASO-treated mice (Fig. 4*C*).

Of note, the LPS response in white adipose tissue–treated mice was unique in CGI-58 ASO-treated mice (Supplementary Fig. 11). In support of this, LPS-induced expression of IL-1β, TNFα, and several other T_H1 cytokines was dramatically elevated in the white adipose tissue of CGI-58 ASO-treated mice compared with that of control mice (Fig. 4*C* and Supplementary Fig. 11; data not shown). In contrast, LPS-driven expression of IL-1β and TNFα was reciprocally diminished in the liver, lung, spleen, and kidney of CGI-58 ASO-treated mice compared with LPS-injected controls (Supplementary Fig. 11). Both white and brown adipose tissue from CGI-58 ASO-treated mice had four- to sevenfold higher expression of the macrophage marker CD-68 (Supplementary Fig. 11).

We surmised that the integrated inflammatory response to endotoxin was dramatically altered by CGI-58 KD (Fig. 4 and Supplementary Fig. 11). However, we were concerned that this effect may be simply a result of the abnormally high accumulation of TAGs in the liver of CGI-58 ASO-treated mice (2) (Supplementary Fig. 1). To rule out this possibility, we fed mice an HFD for 4 weeks, which increased hepatic TAG levels to the same levels seen in chow-fed CGI-58

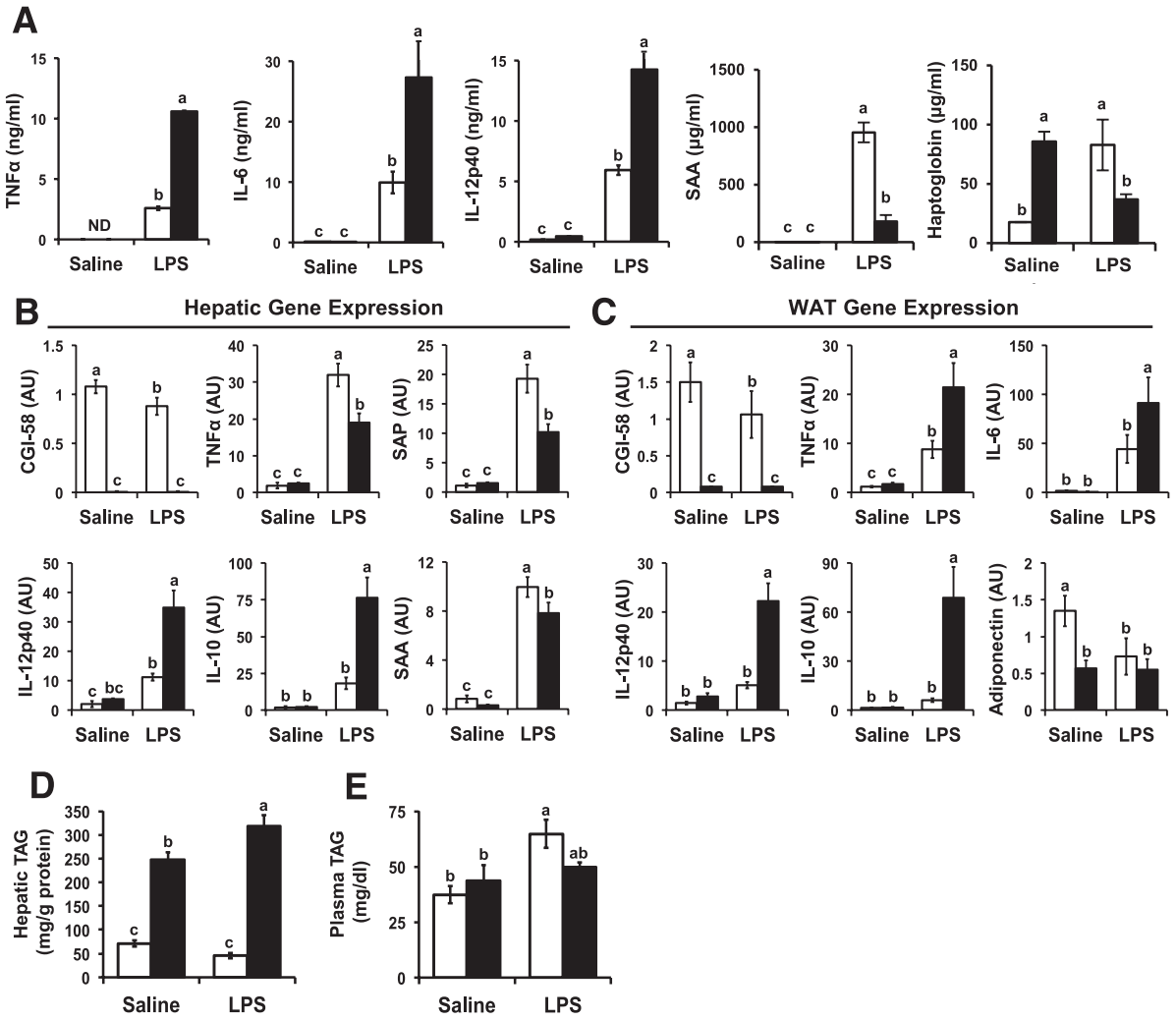

FIG. 4. CGI-58 KD alters the systemic inflammatory and metabolic response to endotoxin. C57BL/6N mice were fed a standard chow diet in conjunction with biweekly injections of a nontargeting control ASO (□) or CGI-58 ASO (■) for 4 weeks. Thereafter, mice received a single intraperitoneal injection of either saline or LPS (5 μg/mouse) and were necropsied 6 h after injection. *A*: Plasma cytokine and acute-phase response protein levels were measured at 1 h (for TNFα only) and 6 h after injection (for IL-6 and IL-12p40 and for SAA and haptoglobin). ND, levels below limit of detection. *B* and *C*: qPCR analyses of hepatic (*B*) and epididymal adipose tissue (*C*) gene expression. SAP, serum amyloid P-component. WAT, white adipose tissue. *D*: Hepatic TAG levels. *E*: Plasma TAG levels at 6 h after injection. Data in *A*, *D*, and *E* represent the mean ± SEM (n = 6), and qPCR data in *B* and *C* represent the mean ± SEM (n = 5). Within each panel, values not sharing a common superscript letter differ significantly ($P < 0.05$). AU, arbitrary unit.

ASO-treated mice (Supplementary Fig. 12*B*). We then treated these HFD-fed mice with LPS to determine whether HFD-induced fatty liver could alter the acute-phase response in a similar fashion to CGI-58 ASO treatment. Of importance, HFD feeding did not mimic the effects of CGI-58 KD on LPS-driven plasma cytokine levels (Supplementary Fig. 12*C* and *D*) or the hepatic acute-phase response (Supplementary Fig. 12*E*). Moreover, CGI-58 ASO treatment increased plasma T_H1 cytokines and blunted the acute-phase response of mice on both chow and HFDs (Supplementary Fig. 12*C*–*E*), further supporting the idea that CGI-58 ASO-driven alteration in inflammatory signaling is an on-target effect of the ASO and not a result of hepatic TAG accumulation.

Given CGI-58's documented role in promoting adipose lipolysis (1) and hepatic VLDL-TAG packaging (2), we examined these parameters in LPS-injected, CGI-58 ASO-treated mice. LPS treatment increased plasma nonesterified fatty acid levels by 18% in chow-fed control ASO-treated mice and 25% in chow-fed CGI-58 ASO-treated mice, indicating that LPS-driven adipose lipolysis was similar between groups (data not shown). However, in these same mice, the hepatic metabolic response to LPS was altered (Fig. 4*D* and *E*). LPS treatment of chow-fed CGI-58 ASO-treated mice resulted in a significant (29%) increase in hepatic TAG levels (Fig. 4*D*) but no comparable change in control ASO-treated mice. Of interest, LPS treatment caused a 73% increase in plasma TAG levels in chow-fed control ASO-treated mice yet caused no hypertriglyceridemia in CGI-58 ASO-treated mice (Fig. 4*E*). These data suggest that hepatic CGI-58 plays a critical role in the overproduction of TAG-rich lipoproteins during infection. Collectively, these data suggest that CGI-58 function is critical to both the inflammatory and metabolic response to acute infection.

DISCUSSION

Although it generally is accepted that CGI-58 indirectly regulates TAG metabolism by coactivating ATGL (1), we

now alternatively propose that CGI-58's ability to acylate LPA (3,4) also plays a critical role in CGI-58's ability to modulate TAG metabolism and insulin signaling. The major findings of the current study are that CGI-58 KD in mice *1*) improves insulin signaling in liver and skeletal muscle; *2*) prevents HFD-induced stress kinase activation; *3*) prevents the generation of PA and other glycerophospholipid species in response to TNFα, thereby attenuating downstream signaling; and *4*) alters the integrated inflammatory response to endotoxin. In our current working model (Fig. 5), we propose that downstream of hepatic cytokine receptor activation, in response to inflammatory stimuli such as an HFD or LPS treatment, CGI-58 generates signaling lipids either directly through direct acylation of LPA or indirectly by coactivating ATGL-mediated TAG hydrolysis. CGI-58–generated PA, and likely other signaling lipids, can subsequently act as lipid second messengers to activate stress kinases such IKK-β, S6K1, and mTOR. These stress kinases can then facilitate serine phosphorylation of critical residues on IRS-1, thereby dampening hepatic insulin signaling (Fig. 5). This role in cytokine signaling may partially explain why CGI-58 KD causes severe hepatic lipid insult and yet improves hepatic insulin signaling.

It has now been a decade since the causal link between CGI-58 mutations and CDS was established (5), yet molecular mechanism(s) by which CGI-58 prevents CDS has remained elusive. Early studies using skin fibroblasts isolated from patients with neutral lipid storage disease or CDS showed that these cultured cells had striking accumulation of intracellular TAGs under normal growth conditions (10,11,38–41). However, the TAG accumulation could not be explained by alteration in mitochondrial fatty acid uptake, β-oxidation, in vitro lipase activity, or TAG synthesizing enzyme activity (10,11,38–41). Instead, it was found that neutral lipid storage disease fibroblasts had impaired turnover of long-chain fatty acids from stored TAGs (38–41). We have likewise demonstrated that targeted knockdown of CGI-58 in hepatocytes impairs intracellular TAG hydrolysis in vitro and in vivo (2,42). Of interest, CGI-58 is a lipid-droplet–associated protein in adipocytes, achieving this subcellular localization by directly interacting with perilipin A (43,44). However, it is important to note that CGI-58 is not always associated with lipid droplets in nonadipocyte cell models (42–44), and the intracellular trafficking itinerary of CGI-58 under hormonal or cytokine stimulation deserves further study.

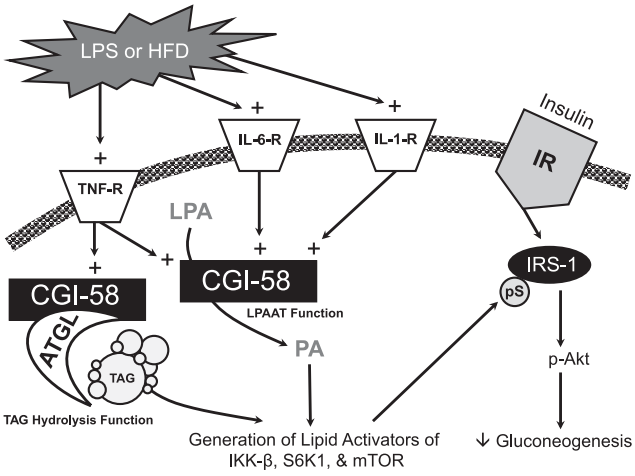

FIG. 5. Proposed model for CGI-58's integrated role in inflammatory responses and insulin action in the liver. In response to inflammatory stimuli, such as an HFD or LPS, plasma levels of inflammatory cytokines, such TNFα, IL-1β, and IL-6, are increased. These inflammatory cytokines normally signal through their membrane-bound receptors (TNF-R, IL-6-R, and IL-1-R) to promote CGI-58–driven generation of signaling lipids either directly from LPAAT activity or indirectly by coactivating ATGL to generate lipid signals from TAG hydrolysis. CGI-58–generated PA, and likely other signaling lipids, can subsequently act as a critical second messenger to promote the activation of inflammatory stress kinases, such as IKK-β, S6K1, and mTOR. Collectively, these activated stress kinases (IKK-β, S6K1, and mTOR) can facilitate serine phosphorylation (pS) of critical serine residues (Ser307, Ser612, Ser632, and Ser1101) on IRS-1, thereby dampening hepatic insulin signaling. Knocking down CGI-58 diminishes this potent negative regulatory loop, thereby improving hepatic insulin action. IR, insulin receptor. TNF-R, TNF receptor.

The product of the LPAAT reaction, PA, is a well-studied signaling lipid (7–9,45–47). In fact, PA participates in many cellular signal transduction pathways and regulates membrane trafficking (7–9,45–47). It is generally accepted that PA regulates cell signaling by physically interacting with target proteins through defined PA-binding motifs, thereby altering either membrane localization or activation state. Bona fide PA-binding proteins include protein kinases, phosphatases, phosphodiesterases, scaffolding proteins, and small guanine nucleotide exchange factors (7–9,45–47). Although the majority of acute cytokine-stimulated PA generation has been attributed to the enzymatic hydrolysis of PC through the action of phospholipase D (45–47) or the phosphorylation of DAGs by DAG kinases (48), there is growing evidence that LPAAT enzymes make substantial contributions to endotoxin- and cytokine-stimulated PA generation (29–33). In fact, pharmacologic inhibition of LPAAT activity protects mice against endotoxic shock, lung injury, and pancreatic islet dysfunction in response to endotoxin and IL-1 (32,33,49,50), implicating LPAAT-derived PA in promoting inflammatory disease. Undoubtedly, PA is a central lipid signaling molecule that can be synthesized or broken down by a number of enzymatic pathways (45–50). We propose that CGI-58–driven synthesis of PA represents a novel lipid-signaling pathway that may have important implications in human diseases, such as the metabolic syndrome and CDS. CGI-58 KD in mice prevents diet-induced obesity and decreases fat-pad mass (2), suggesting a defect in lipid storage by adipose tissue. The possibility that CGI-58–generated signaling lipids may regulate adipocyte function in vivo deserves further investigation. The signaling function of CGI-58 may also have implications for neurologic defects in CDS, including ataxia, mental retardation, and hearing loss. Given that global deficiency of CGI-58 results in postnatal lethality, tissue-specific CGI-58 knockout mice will be required to further dissect the role of CGI-58–generated signaling lipids in these other biological processes. In conclusion, these studies demonstrate that CGI-58 is a novel source of signaling lipids that integrate inflammation and nutrient metabolism.

ACKNOWLEDGMENTS

This work was supported by the Department of Pathology at Wake Forest University and by grants from the American Heart Association (grant 11BGIA7840072 to J.M.B.); the National Heart, Lung, and Blood Institute (grants 1-K99-HL-096166 to J.M.B., 5-T32-HL-091796 to C.C.L., and 5-P01-HL-049373 to J.S.P.); the National Institute of Diabetes and Digestive and Kidney Diseases (grants 1-F32-DK-084582 to J.L.B. and 1-R01-054797 to D.L.B.); the National Institute of

General Medical Sciences LIPID MAPS (grant U54-GM-069338 to H.A.B.); and the Intramural Research Program of the National Institute of Environmental Health Sciences (grant NIEHS Z01-ES-102005 to M.B.F.).

No potential conflicts of interest relevant to this article were reported.

C.C.L., J.L.B., G.T., and M.A.D. conducted the experiments, analyzed the data, and aided in the manuscript preparation. P.T.I., S.B.M., D.S.M., and H.A.B. performed all lipidomic analyses and provided critical insights for these studies. S.C., M.L., and J.S.P. performed primary hepatocyte isolations. R.G.L., R.M.C., and M.J.G. provided antisense oligonucleotides and valuable discussion. D.L.B. aided in the measurements of hepatic LPAAT activity. M.B.F. and J.M. performed plasma cytokine analyses and discussed the data. J.M.B. planned the project, designed the experiments, analyzed the data, wrote the manuscript, and is the guarantor of this work and, as such, had full access to all the data in the study and takes responsibility for the integrity of the data and the accuracy of the data analysis. All authors were involved in the editing of the final manuscript.

The authors thank all members of the laboratories of J.M.B. (Wake Forest University School of Medicine), Ryan Temel (Wake Forest University School of Medicine), Larry Rudel (Wake Forest University School of Medicine), and Paul Dawson (Wake Forest University School of Medicine) for comments and suggestions. The authors also thank Deanna Russell (Rutgers University) for technical assistance.

REFERENCES

1. Lass A, Zimmermann R, Haemmerle G, et al. Adipose triglyceride lipase-mediated lipolysis of cellular fat stores is activated by CGI-58 and defective in Chanarin-Dorfman Syndrome. Cell Metab 2006;3:309–319
2. Brown JM, Betters JL, Lord C, et al. CGI-58 knockdown in mice causes hepatic steatosis but prevents diet-induced obesity and glucose intolerance. J Lipid Res 2010;51:3306–3315
3. Montero-Moran G, Caviglia JM, McMahon D, et al. CGI-58/ABHD5 is a coenzyme A-dependent lysophosphatidic acid acyltransferase. J Lipid Res 2010;51:709–719
4. Ghosh AK, Ramakrishnan G, Chandramohan C, Rajasekharan R. CGI-58, the causative gene for Chanarin-Dorfman syndrome, mediates acylation of lysophosphatidic acid. J Biol Chem 2008;283:24525–24533
5. Lefèvre C, Jobard F, Caux F, et al. Mutations in CGI-58, the gene encoding a new protein of the esterase/lipase/thioesterase subfamily, in Chanarin-Dorfman syndrome. Am J Hum Genet 2001;69:1002–1012
6. Radner FP, Streith IE, Schoiswohl G, et al. Growth retardation, impaired triacylglycerol catabolism, hepatic steatosis, and lethal skin barrier defect in mice lacking comparative gene identification-58 (CGI-58). J Biol Chem 2010;285:7300–7311
7. Wymann MP, Schneiter R. Lipid signalling in disease. Nat Rev Mol Cell Biol 2008;9:162–176
8. Hla T, Lee MJ, Ancellin N, Paik JH, Kluk MJ. Lysophospholipids: receptor revelations. Science 2001;294:1875–1878
9. Fang Y, Vilella-Bach M, Bachmann R, Flanigan A, Chen J. Phosphatidic acid-mediated mitogenic activation of mTOR signaling. Science 2001;294:1942–1945
10. Igal RA, Coleman RA. Acylglycerol recycling from triacylglycerol to phospholipid, not lipase activity, is defective in neutral lipid storage disease fibroblasts. J Biol Chem 1996;271:16644–16651
11. Williams ML, Coleman RA, Placezk D, Grunfeld C. Neutral lipid storage disease: a possible functional defect in phospholipid-linked triacylglycerol metabolism. Biochim Biophys Acta 1991;1096:162–169
12. Crooke RM, Graham MJ, Lemonidis KM, Whipple CP, Koo S, Perera RJ. An apolipoprotein B antisense oligonucleotide lowers LDL cholesterol in hyperlipidemic mice without causing hepatic steatosis. J Lipid Res 2005;46:872–884
13. Brown JM, Boysen MS, Chung S, et al. Conjugated linoleic acid induces human adipocyte delipidation: autocrine/paracrine regulation of MEK/ERK signaling by adipocytokines. J Biol Chem 2004;279:26735–26747
14. Brown JM, Chung S, Sawyer JK, et al. Inhibition of stearoyl-coenzyme A desaturase 1 dissociates insulin resistance and obesity from atherosclerosis. Circulation 2008;118:1467–1475
15. Brown JM, Bell TA 3rd, Alger HM, et al. Targeted depletion of hepatic ACAT2-driven cholesterol esterification reveals a non-biliary route for fecal neutral sterol loss. J Biol Chem 2008;283:10522–10534
16. Ivanova PT, Milne SB, Byrne MO, Xiang Y, Brown HA. Glycerophospholipid identification and quantitation by electrospray ionization mass spectrometry. Methods Enzymol 2007;432:21–57
17. Chung S, Timmins JM, Duong M, et al. Targeted deletion of hepatocyte ABCA1 leads to very low density lipoprotein triglyceride overproduction and low density lipoprotein hypercatabolism. J Biol Chem 2010;285:12197–12209
18. Draper DW, Madenspacher JH, Dixon D, King DH, Remaley AT, Fessler MB. ATP-binding cassette transporter G1 deficiency dysregulates host defense in the lung. Am J Respir Crit Care Med 2010;182:404–412
19. Lowry OH, Rosebrough NJ, Farr AL, Randall RJ. Protein measurement with the Folin phenol reagent. J Biol Chem 1951;193:265–275
20. Bligh EG, Dyer WJ. A rapid method of total lipid extraction and purification. Can J Biochem Physiol 1959;37:911–917
21. Callender HL, Forrester JS, Ivanova P, Preininger A, Milne S, Brown HA. Quantification of diacylglycerol species from cellular extracts by electrospray ionization mass spectrometry using a linear regression algorithm. Anal Chem 2007;79:263–272
22. Erion DM, Shulman GI. Diacylglycerol-mediated insulin resistance. Nat Med 2010;16:400–402
23. Hotamisligil GS, Peraldi P, Budavari A, Ellis R, White MF, Spiegelman BM. IRS-1-mediated inhibition of insulin receptor tyrosine kinase activity in TNF-alpha- and obesity-induced insulin resistance. Science 1996;271:665–668
24. Yuan M, Konstantopoulos N, Lee J, et al. Reversal of obesity- and diet-induced insulin resistance with salicylates or targeted disruption of Ikkbeta. Science 2001;293:1673–1677
25. Arkan MC, Hevener AL, Greten FR, et al. IKK-beta links inflammation to obesity-induced insulin resistance. Nat Med 2005;11:191–198
26. Um SH, Frigerio F, Watanabe M, et al. Absence of S6K1 protects against age- and diet-induced obesity while enhancing insulin sensitivity. Nature 2004;431:200–205
27. Fingar DC, Blenis J. Target of rapamycin (TOR): an integrator of nutrient and growth factor signals and coordinator of cell growth and cell cycle progression. Oncogene 2004;23:3151–3171
28. Hirosumi J, Tuncman G, Chang L, et al. A central role for JNK in obesity and insulin resistance. Nature 2002;420:333–336
29. Tong W, Shah D, Xu J, et al. Involvement of lipid mediators on cytokine signaling and induction of secretory phospholipase A2 in immortalized astrocytes (DITNC). J Mol Neurosci 1999;12:89–99
30. Bursten SL, Harris WE, Bomsztyk K, Lovett D. Interleukin-1 rapidly stimulates lysophosphatidate acyltransferase and phosphatidate phosphohydrolase activities in human mesangial cells. J Biol Chem 1991;266:20732–20743
31. Bursten SL, Harris WE, Resch K, Lovett DH. Lipid A activation of glomerular mesangial cells: mimicry of the bioactive lipid, phosphatidic acid. Am J Physiol 1992;262:C328–C338
32. Rice GC, Brown PA, Nelson RJ, Bianco JA, Singer JW, Bursten S. Protection from endotoxic shock in mice by pharmacologic inhibition of phosphatidic acid. Proc Natl Acad Sci USA 1994;91:3857–3861
33. Abraham E, Bursten S, Shenkar R, et al. Phosphatidic acid signaling mediates lung cytokine expression and lung inflammatory injury after hemorrhage in mice. J Exp Med 1995;181:569–575
34. Hardardóttir I, Grünfeld C, Feingold KR. Effects of endotoxin and cytokines on lipid metabolism. Curr Opin Lipidol 1994;5:207–215
35. Shindou H, Hishikawa D, Harayama T, Yuki K, Shimizu T. Recent progress on acyl CoA: lysophospholipid acyltransferase research. J Lipid Res 2009;50(Suppl.):S46–S51
36. Barton GM. A calculated response: control of inflammation by the innate immune system. J Clin Invest 2008;118:413–420
37. Nathan C. Points of control in inflammation. Nature 2002;420:846–852
38. Williams ML, Monger DJ, Rutherford SL, Hincenbergs M, Rehfeld SJ, Grunfeld C. Neutral lipid storage disease with ichthyosis: lipid content and metabolism of fibroblasts. J Inherit Metab Dis 1988;11:131–143
39. Hilaire N, Nègre-Salvayre A, Salvayre R. Cytoplasmic triacylglycerols and cholesteryl esters are degraded in two separate catabolic pools in cultured human fibroblasts. FEBS Lett 1993;328:230–234
40. Hilaire N, Nègre-Salvayre A, Salvayre R. Cellular uptake and catabolism of high-density-lipoprotein triacylglycerols in human cultured fibroblasts: degradation block in neutral lipid storage disease. Biochem J 1994;297:467–473

41. Hilaire N, Salvayre R, Thiers JC, Bonnafé MJ, Nègre-Salvayre A. The turnover of cytoplasmic triacylglycerols in human fibroblasts involves two separate acyl chain length-dependent degradation pathways. J Biol Chem 1995;270:27027–27034
42. Brown JM, Chung S, Das A, Shelness GS, Rudel LL, Yu L. CGI-58 facilitates the mobilization of cytoplasmic triglyceride for lipoprotein secretion in hepatoma cells. J Lipid Res 2007;48:2295–2305
43. Subramanian V, Rothenberg A, Gomez C, et al. Perilipin A mediates the reversible binding of CGI-58 to lipid droplets in 3T3-L1 adipocytes. J Biol Chem 2004;279:42062–42071
44. Yamaguchi T, Omatsu N, Matsushita S, Osumi T. CGI-58 interacts with perilipin and is localized to lipid droplets: possible involvement of CGI-58 mislocalization in Chanarin-Dorfman syndrome. J Biol Chem 2004;279:30490–30497
45. Jenkins GM, Frohman MA. Phospholipase D: a lipid centric review. Cell Mol Life Sci 2005;62:2305–2316
46. Andresen BT, Rizzo MA, Shome K, Romero G. The role of phosphatidic acid in the regulation of the Ras/MEK/Erk signaling cascade. FEBS Lett 2002;531:65–68
47. Exton JH. Phospholipase D: enzymology, mechanisms of regulation, and function. Physiol Rev 1997;77:303–320
48. Topham MK, Epand RM. Mammalian diacylglycerol kinases: molecular interactions and biological functions of selected isoforms. Biochim Biophys Acta 2009;1790:416–424
49. Bleich D, Chen S, Bursten SL, Nadler JL. Lisofylline, an inhibitor of unsaturated phosphatidic acid generation, ameliorates interleukin-1 beta-induced dysfunction in cultured rat islets. Endocrinology 1996;137:4871–4877
50. Guidot DM, Bursten SL, Rice GC, et al. Modulating phosphatidic acid metabolism decreases oxidative injury in rat lungs. Am J Physiol 1997;273:L957–L966